atmosphere

MDPI

Article

Distribution of Fine Particulate Matter Pollution in Winter over Eastern China Affected by Synoptic Conditions

Xiaohui Liu [1,2], Huafeng Wu [1,*], Youjia Zou [1] and Pinya Wang [2]

[1] Merchant Marine Academy, Shanghai Maritime University, Shanghai 201306, China; xhliu@shmtu.edu.cn (X.L.); yjzou@shmtu.edu.cn (Y.Z.)
[2] Collaborative Innovation Center of Atmospheric Environment and Equipment Technology, Jiangsu Key Laboratory of Atmospheric Environment Monitoring and Pollution Control (AEMPC), Nanjing University of Information Science & Technology, Nanjing 210044, China
* Correspondence: hfwu@shmtu.edu.cn

Abstract: Based on the mean sea level pressure field and 10-meter wind field across eastern China, weather patterns were classified using principal component analysis in the T-model (T-PCA), and four weather conditions were identified. Weather conditions and meteorological factors affecting the winter $PM_{2.5}$ concentration in the Beijing–Tianjin–Hebei (BTH) region and the Yangtze River Delta (YRD) were also analyzed. The results showed that there were significant differences in the $PM_{2.5}$ distribution between BTH and the YRD under different weather conditions. The intensity and path of cold air played important roles in regulating the $PM_{2.5}$ concentration distribution in eastern China. For the BTH region, under type 2 and type 4 conditions, the weather was stable, and heavy pollution frequently occurred; however, under type 1 and type 3 conditions, cold air was active, and the air quality improved. For the YRD, both type 1 and type 4 conditions lead to high $PM_{2.5}$ concentrations in this region. Type 1 cold air flows southward along the northwestern path and is beneficial for transporting pollutants from BTH to the YRD, causing a high probability of $PM_{2.5}$ pollution. Conversely, the southward movement of type 3 cold air along the eastern path was beneficial for pollutant diffusion in the YRD.

Keywords: synoptic patterns; meteorological conditions; $PM_{2.5}$ pollution difference; Beijing–Tianjin–Hebei; Yangtze River Delta

check for updates

Citation: Liu, X.; Wu, H.; Zou, Y.; Wang, P. Distribution of Fine Particulate Matter Pollution in Winter over Eastern China Affected by Synoptic Conditions. *Atmosphere* **2024**, *15*, 821. https://doi.org/10.3390/atmos15070821

Academic Editors: Pavel Kishcha, Célia Alves and Anthony R. Lupo

Received: 17 February 2024
Revised: 8 May 2024
Accepted: 3 July 2024
Published: 8 July 2024

Copyright: © 2024 by the authors. Licensee MDPI, Basel, Switzerland. This article is an open access article distributed under the terms and conditions of the Creative Commons Attribution (CC BY) license (https://creativecommons.org/licenses/by/4.0/).

1. Introduction

Wintertime fine particulate matter ($PM_{2.5}$) pollution in China has attracted worldwide attention in recent years [1–6]. Heavy $PM_{2.5}$ pollution easily causes reduced visibility and has adverse impacts on human health, including increased death and morbidity from lung cancer [7,8]. Since the "Air Pollution Prevention and Control Action Plan" was implemented in 2013, the annual average $PM_{2.5}$ concentration has significantly decreased [9–12]. However, heavy $PM_{2.5}$ pollution with high concentrations still frequently occurs over eastern China [13]. For example, the maximum $PM_{2.5}$ concentration reached 731 $\mu g/m^3$ in the winter of 2016 [14]. Therefore, $PM_{2.5}$ represents a major environmental problem in winter in China.

Regional $PM_{2.5}$ pollution is affected by complex interactions among pollution sources, atmospheric chemical processes [15], and meteorological conditions [16–19]. High anthropogenic emissions are the underlying cause of $PM_{2.5}$ pollution, while regional $PM_{2.5}$ pollution events generally occur under weather conditions that are conducive to the formation and accumulation of air pollutants, such as weak wind speeds [20,21] and low boundary layer heights (PBLs) [22–25], seriously inhibiting the diffusion of air pollutants and resulting in the accumulation of pollutants [26].

$PM_{2.5}$ pollution events typically occur during winter in Beijing–Tianjin–Hebei (BTH) and the Yangtze River Delta (YRD) in eastern China. Many studies have been conducted to

explore the causes of $PM_{2.5}$ pollution in these two regions [17,27,28]. Regional persistent haze events in BTH often occur during stable weather. These fluctuations can be categorized into two types according to the large-scale circulation, i.e., the zonal westerly airflow type and the high-pressure ridge type [29]. These two circulation situations were favorable for airflow sinking motion, reducing the PBL, thus preventing air pollutants from diffusing upward and facilitating the occurrence of haze events [30]. In addition to stable weather, $PM_{2.5}$ pollution in the YRD was significantly impacted by upstream transport effects. Kang et al. [31] noted that in the YRD, the amount of $PM_{2.5}$ mass transported from the North China Plain (NCP) was 10–15 times greater during cold front episodes.

Huang et al. [32] revealed that long-range transport and aerosol–boundary layer feedback between BTH and the YRD could enhance inter-regional pollution. Based on our previous study [33], we also found a seesaw pattern of interannual $PM_{2.5}$ anomalies between BTH and the YRD, especially during strong East Asian winter monsoon years. Generally, in winter, eastern China was controlled by a persistent weak southerly wind conducive to the heterogeneous chemical reaction of aerosols, leading to severe haze in BTH, while the cold front associated with strong northerly wind could reverse local air pollutants over BTH but transport air pollutants to the YRD. Therefore, there were obvious differences in the $PM_{2.5}$ distribution in eastern China in winter that were affected by synoptic conditions.

However, many studies have focused mainly on the influence of synoptic conditions on local $PM_{2.5}$ pollution in BTH or the YRD, and very little research has linked these two regions together, combining synoptic conditions to discuss the impact of meteorological conditions on $PM_{2.5}$ in these two regions [26]. In this study, the weather conditions and meteorological factors affecting $PM_{2.5}$ distribution in BTH and the YRD during the winter from 2013 to 2019 were analyzed. Our results may provide a theoretical basis for the implementation of cross-regional coordinated control of air pollution in BTH and the YRD.

2. Data and Methods

2.1. Data

In this study, we focused on two polluted regions, BTH (36–43° N, 114–120° E) and the YRD (29.5–33.5° N, 118–122.5° E) (Figure 1). Meteorological variable information from winters during 2013–2019 was retrieved from the European Centre for Medium-Range Weather Forecasts' Reanalysis v5 (ERA5) data, with spatial and temporal resolutions of 0.25° × 0.25° and 1 h, respectively. The wintertime sea level pressure fields and the wind at 10 m above ground level were used to classify synoptic patterns. The surface and high temperature, wind and relative humidity fields and PBL were used to calculate meteorological factors.

The daily $PM_{2.5}$ concentrations during winters from 2013 to 2019 were obtained from the China High $PM_{2.5}$ dataset (https://weijing-rs.github.io/product.html) (accessed on 1 January 2024). The $PM_{2.5}$ dataset was generated by the Moderate Resolution Imaging Spectroradiometer (MODIS) and Multiangle Implementation of Atmospheric Correction (MAIAC) algorithm combined with the Space–Time Extra-Trees (STET) model, with temporal resolutions of 1 km × 1 km [34]. We interpolated the spatial resolution of $PM_{2.5}$ to 0.25° × 0.25° to ensure spatial resolution continuity between $PM_{2.5}$ and the meteorological factors.

2.2. Methods

We utilized the temperature and wind fields at the 1000 hPa, 925 hPa, and 850 hPa levels; the PBL; and relative humidity at 1000 hPa provided by ERA5 data to calculate the main atmospheric dynamic and thermodynamic meteorological factors affecting $PM_{2.5}$. Based on our previous study [17], we calculated the correlation coefficients (R) between meteorological factors and $PM_{2.5}$ and selected $R > 0.3$ ($p < 0.01$) as the main meteorological factors. The ventilation coefficient (Ven) for the PBL, meridional wind at 850 hPa (V_{850}) and the PBL as the main atmospheric dynamics factors affecting $PM_{2.5}$, as well as the

temperature at 850 hPa (T_{850}), the temperature difference between 925 hPa and 1000 hPa ($T_{925–1000}$) and the corresponding difference in the pseudoadiabatic potential temperature ($\theta_{se_925–1000}$), were selected as the main thermodynamic factors.

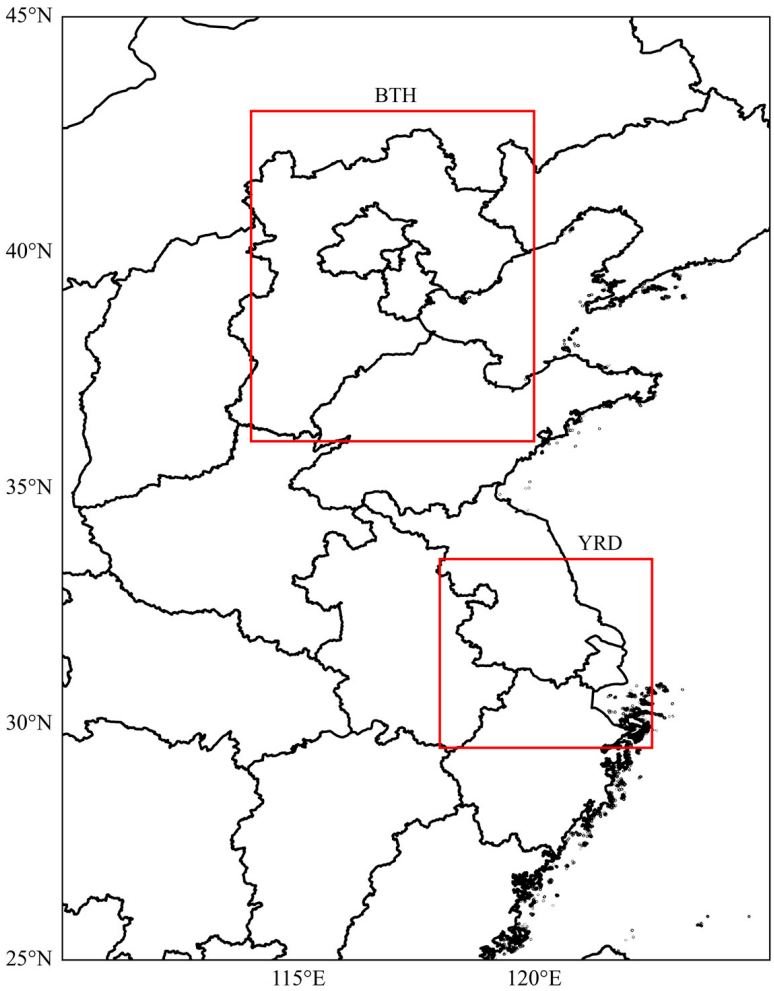


Figure 1. The regional range of BTH and YRD.

Synoptic classification has been widely used to describe and analyze atmospheric circulation and weather conditions. Huth et al. [35] compared various objective classification methods for weather patterns and recommended the use of an obliquely rotated principal component analysis in the T-model (T-PCA). This method can accurately capture the characteristics of the original circulation field, exhibiting minimal changes with adjustments to the classification objects [35,36]. In this study, we applied the T-PCA method to identify the winter sea level pressure fields and 10 m wind fields across eastern China.

3. Results

3.1. Synoptic Pattern Affecting Eastern China

Objective weather classification was performed on the sea level pressure field and 10 m wind field data during winters from 2013 to 2019, with a sample size of 632 days, resulting in the identification of four weather patterns. Figure 2 shows the average sea level pressure and 10 m wind field for each synoptic pattern. The four weather types can be described as follows: type 1—high pressure was located in Siberia, and cold air moved south into eastern China along the northwest path; type 2—the main part of the high pressure was located in Siberia, and a weak high pressure (the center was located in Shandong Province) split from the Siberia high; type 3—high pressure was located in Siberia, and cold air moved

south into eastern China along the northeast path; and type 4—a weak high-pressure field over the Yellow Sea. Eastern China was controlled by uniform pressure and weak winds.

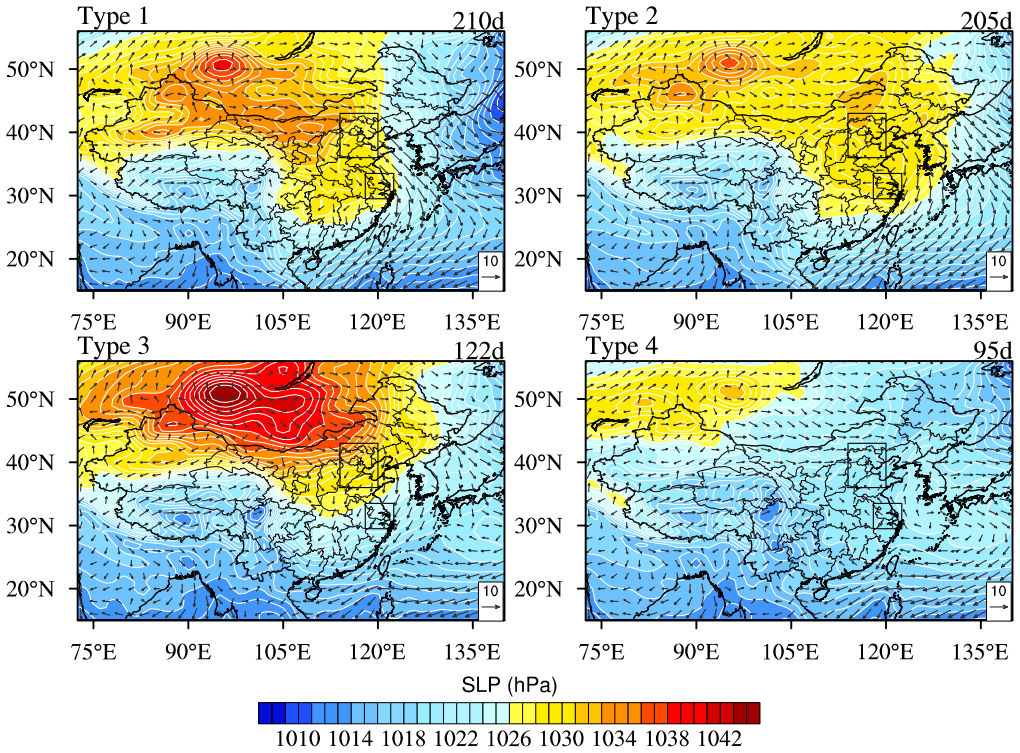


Figure 2. The sea level pressure (SLP; unit: hPa) and winds at 10 m (unit: m/s) in winter from December 2013 to February 2020 for the 4 weather types. The number at the top right corner of each panel indicates the number of days under each weather type. The black frame area on the north side of each panel represents BTH, while the one on the south side represents YRD.

The four weather types accounted for 33.2%, 32.4%, 19.3% and 15.1% of the total number of days, respectively. Type 1 was the most common weather pattern during winter, with the center of the Mongolian high pressure positioned near 50° N, 90° E, and the central intensity was 1040 hPa. The cold air pressure was strong, the sea level pressure of 1028 hPa pressed southward to approximately 25° N, and the cold air flowed along the northwestern path southward. BTH and YRD were located in the front part of the Mongolian high-pressure system, and both regions were controlled by the northwesterly airflow, accompanied by strong western winds. During this type 2 weather, the cold air influence was weak, and the wind speed was low over eastern China. BTH was at the back of the weak high-pressure zone (the center was located in Shandong Province). The YRD was located at the bottom of this weak high-pressure zone and was controlled by northeasterly winds. Type 3 exhibited the highest Mongolian high center intensity at 1044 hPa, and the 1028 hPa was situated near 33° N. Both BTH and the YRD were located in front of the high-pressure zone. Cold air moved southward along the eastern path, with dense isobars and high wind speeds. The area north of BTH experienced a northwestern airflow, while the central and southern parts of BTH and the whole YRD region were influenced mainly by an easterly airflow. Type 4 had the weakest Mongolian high pressure, and the center intensity was only 1030 hPa. The influence range of the Mongolian high pressure was minimal, with the sea level pressure in most parts of China being less than 1024 hPa. A weak high-pressure system was present over the Yellow Sea, and the central strength was less than 1028 hPa. BTH and the YRD were located at the back of the weak high-pressure zone, which had a weak pressure gradient and was affected by weak southerly winds.

3.2. The Influence of Synoptic Patterns on $PM_{2.5}$

3.2.1. $PM_{2.5}$ Distribution over BTH and YRD under Different Synoptic Patterns

Figure 3 shows the $PM_{2.5}$ concentrations under the four weather types in eastern China during winters from 2013 to 2019. Figure 4 summarizes the average $PM_{2.5}$ concentration and frequency distribution of pollution levels in BTH and the YRD under corresponding weather conditions. Under type 1 conditions, cold air passed through the heavily polluted area of the NCP, and air pollutants were easily transported downstream. As shown in Figure 3a, BTH was the cleanest region, and the $PM_{2.5}$ regional average was 53 $\mu g/m^3$, with the lowest frequency of different pollution levels (Figure 4a). The frequency of severe pollution (5%) was significantly lower than that of other weather types (Figure 4a). In contrast, the YRD experienced the heaviest pollution, with $PM_{2.5}$ concentrations ranging from 75 to 100 $\mu g/m^3$, and the $PM_{2.5}$ regional average was 78 $\mu g/m^3$. Type 1 weather conditions were the most conducive to the dispersion of pollutants in BTH; however, these conditions were prone to causing severe pollution in the YRD.

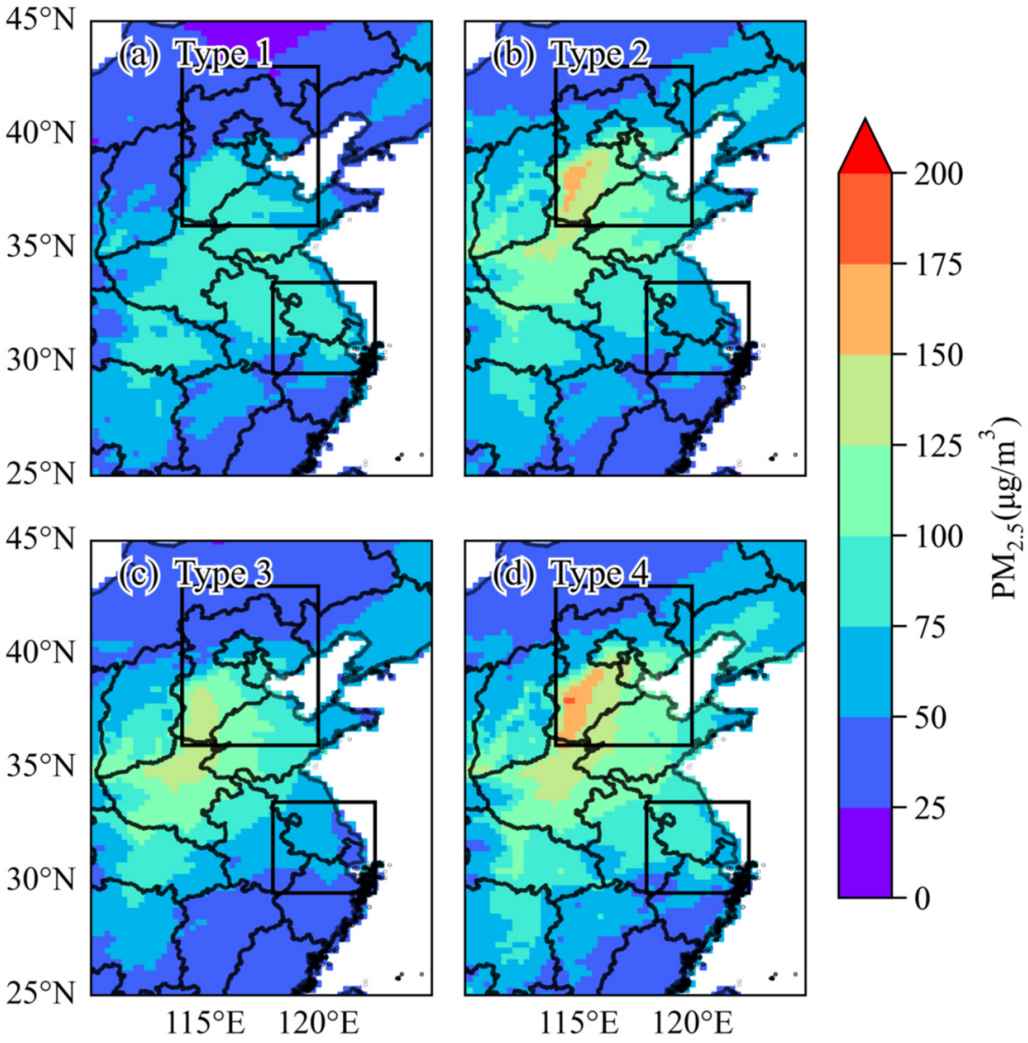


Figure 3. The average $PM_{2.5}$ concentration during the 4 weather types over eastern China: (**a**) type 1; (**b**) type 2; (**c**) type 3; (**d**) type 4. The black frame area on the north side of each panel represents BTH, while the one on the south side represents YRD.

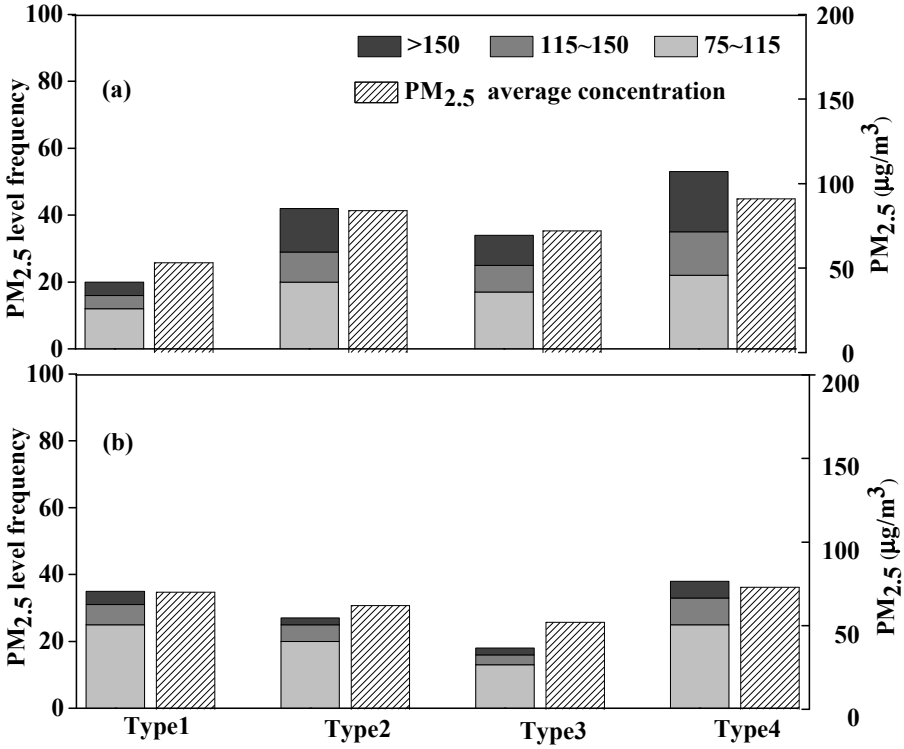


Figure 4. Average $PM_{2.5}$ concentration and frequency of different pollution levels under the four weather types in BTH and the YRD (light pollution: 75 $\mu g/m^3$ < $PM_{2.5}$ ≤ 115 $\mu g/m^3$; moderate pollution: 115 $\mu g/m^3$ < $PM_{2.5}$ ≤ 150 $\mu g/m^3$; severe pollution: $PM_{2.5}$ > 150 $\mu g/m^3$). (**a**) BTH; (**b**) YRD.

Under type 2 conditions, BTH was affected by the weak pressure field at the rear of this high-pressure system, leading to the suppression of the vertical dispersion of atmospheric pollutants. The $PM_{2.5}$ concentration ranged from 46 to 165 $\mu g/m^3$ in BTH. The $PM_{2.5}$ regional average was 84 $\mu g/m^3$ (Figure 4b). The frequencies of light and moderate pollution were 20% and 9%, respectively. The occurrence frequency of severe pollution was 13%, which was consistent with that of type 4 and higher than those of other weather types (Figure 4a). Conversely, the YRD was influenced by an eastward airflow at the front part of the high-pressure system, which was conducive to pollutant dispersion. The $PM_{2.5}$ concentration ranged from 31 to 75 $\mu g/m^3$ (Figure 4b). The $PM_{2.5}$ regional average was 61 $\mu g/m^3$, with 4% and 2% probabilities of moderate and severe pollution, respectively, which were lower than those for the type 1 and type 4 conditions (Figure 4b).

Under type 3 conditions, cold air moves southward along the eastern route, affecting BTH with an eastward airflow, which is conducive to the dispersion of pollutants. The $PM_{2.5}$ concentration ranged from 34 to 146 $\mu g/m^3$ in BTH (Figure 3c). The $PM_{2.5}$ regional average concentration was 97 $\mu g/m^3$, with low frequencies of both light and severe pollution at 18% and 20%, respectively (Figure 4a). In the YRD, the air masses were relatively clean with strong pressure gradients and high eastward wind speeds, resulting in the lowest $PM_{2.5}$ concentration ranging from 26 to 62 $\mu g/m^3$ (Figure 3c). The $PM_{2.5}$ regional average concentration was 52 $\mu g/m^3$, with the lowest frequencies of light, moderate, and severe pollution occurring at 11%, 3%, and 2%, respectively (Figure 4b). Type 3 conditions were the most favorable conditions for pollutant dispersion in the YRD.

For type 4 conditions, the weather was stable with weak south winds. The $PM_{2.5}$ concentration in BTH ranged from 57 to 192 $\mu g/m^3$ (Figure 3d), with the highest regional average concentration of 133 $\mu g/m^3$. The frequencies of light and severe pollution were the highest, accounting for 34% and 24%, respectively (Figure 4a). In the YRD, the $PM_{2.5}$ concentration ranged from 36 to 91 $\mu g/m^3$ (Figure 3d), with a regional average concentration of 76 $\mu g/m^3$. The frequencies of light, moderate, and severe pollution were 25%, 8%, and 6%, respectively. Type 4 represented a typical stagnant weather pattern during winter,

which was the least favorable scenario for the dispersion of air pollutants in both BTH and the YRD.

The $PM_{2.5}$ distributions in BTH and the YRD under different weather conditions revealed that different cold air paths had significant differences in terms of the $PM_{2.5}$ meridional distribution over eastern China. For example, the northwest path cold air (type 1) pushed $PM_{2.5}$ pollution southward, causing high $PM_{2.5}$ concentrations in the YRD, and the eastern path cold air (type 3) was conducive to low $PM_{2.5}$ concentrations in the YRD and high $PM_{2.5}$ concentrations in BTH. If cold air activity is weak, eastern China experiences southern winds; for example, under type 2 or type 4 weather conditions, $PM_{2.5}$ pollution is more likely to occur in BTH.

3.2.2. $PM_{2.5}$ Differences over BTH and the YRD under the Same Synoptic Type

Cold air paths affected the $PM_{2.5}$ distribution over BTH and the YRD. To analyze the difference in $PM_{2.5}$ concentrations between BTH and the YRD, we divided the $PM_{2.5}$ concentration into four patterns under the same weather conditions: $PM_{2.5}$ pattern I—BTH and the YRD were simultaneously clean ($PM_{2.5} < 75$ μg/m^3); $PM_{2.5}$ pattern II—BTH and the YRD were both polluted ($PM_{2.5} > 75$ μg/m^3); $PM_{2.5}$ pattern III—BTH was polluted ($PM_{2.5} > 75$ μg/m^3), while the YRD was clean ($PM_{2.5} < 75$ μg/m^3); and $PM_{2.5}$ pattern IV—BTH was clean ($PM_{2.5} < 75$ μg/m^3), while the YRD was polluted ($PM_{2.5} > 75$ μg/m^3). Figures 5–12 show the distributions of the pressure fields and 10 m wind fields for the four $PM_{2.5}$ patterns and the corresponding $PM_{2.5}$ distributions in BTH and the YRD.

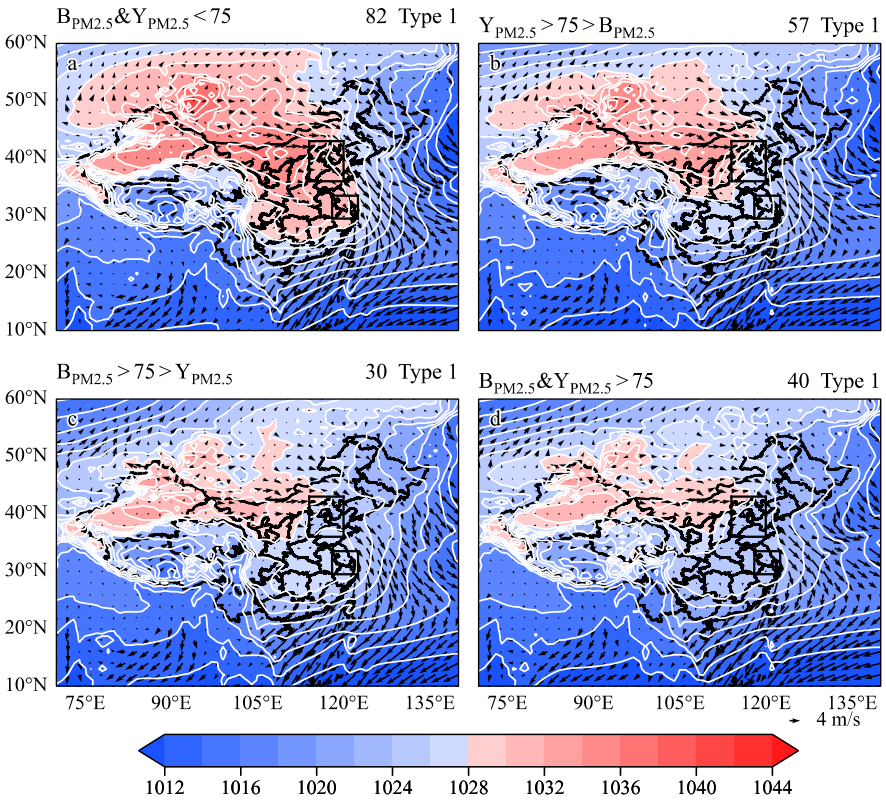


Figure 5. The sea level pressure field and 10 m wind field distribution with different $PM_{2.5}$ patterns under type 1 weather conditions: (**a**) $PM_{2.5}$ pattern I; (**b**) $PM_{2.5}$ pattern II; (**c**) $PM_{2.5}$ pattern III; (**d**) $PM_{2.5}$ pattern IV. The number at the top right corner of each panel indicates the number of days under each $PM_{2.5}$ pattern. The black frame area on the north side of each panel represents BTH, while the one on the south side represents YRD.

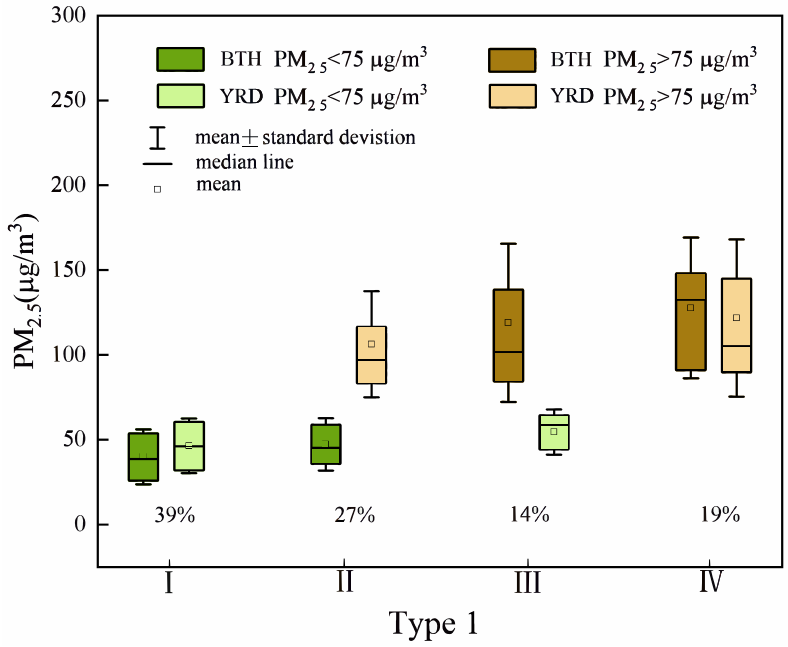


Figure 6. Boxplots of the four $PM_{2.5}$ patterns under type 1 weather conditions.

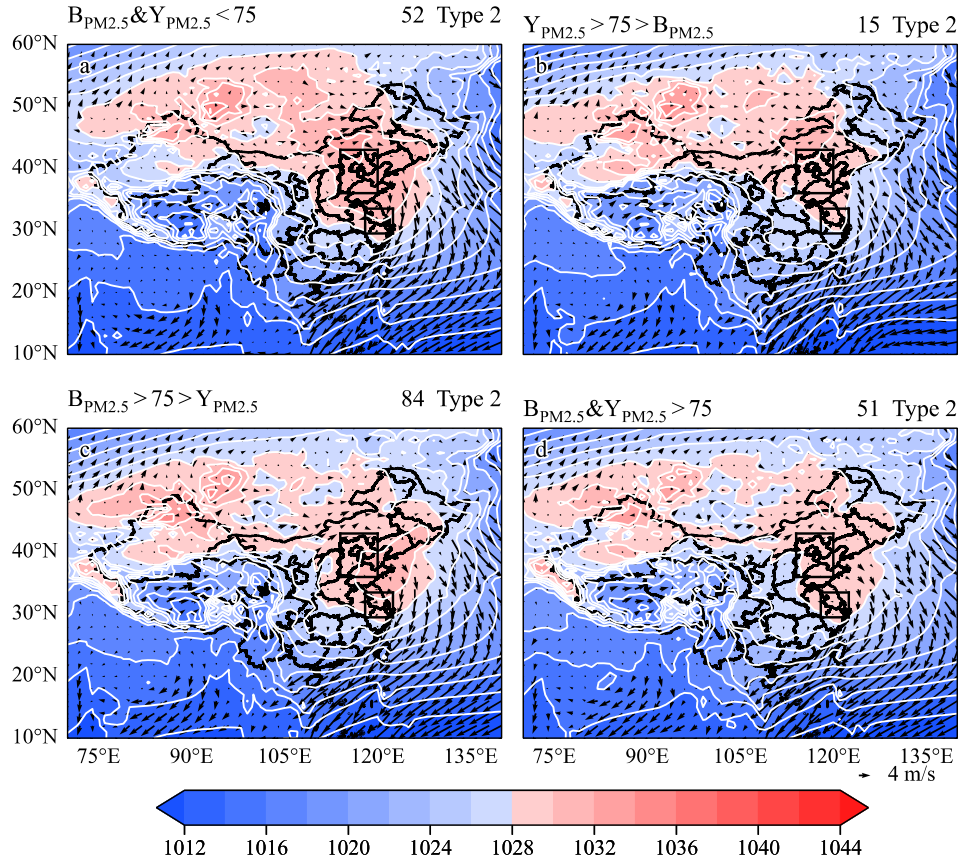


Figure 7. The sea level pressure field and 10 m wind field distribution with different $PM_{2.5}$ patterns under type 2 weather conditions: (**a**) $PM_{2.5}$ pattern I; (**b**) $PM_{2.5}$ pattern II; (**c**) $PM_{2.5}$ pattern III; (**d**) $PM_{2.5}$ pattern IV. The number at the top right corner of each panel indicates the number of days under each $PM_{2.5}$ pattern. The black frame area on the north side of each panel represents BTH, while the one on the south side represents YRD.

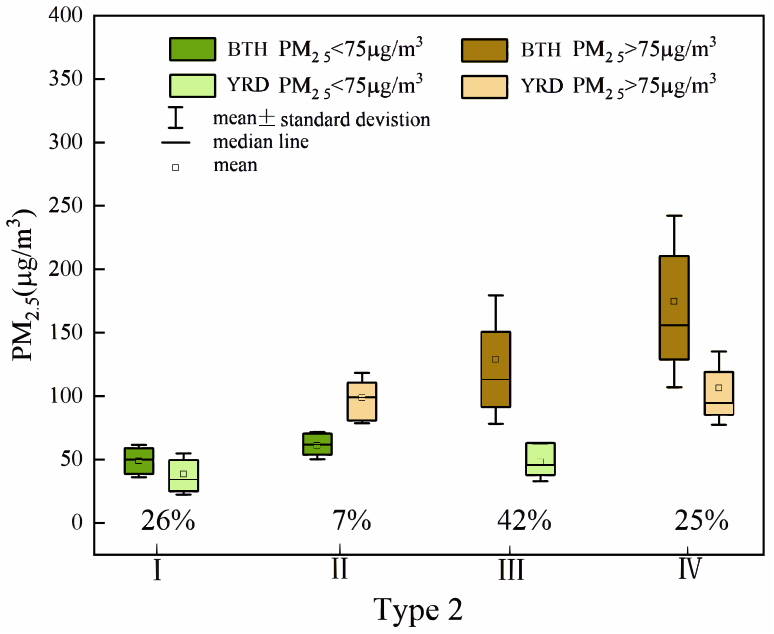


Figure 8. The same as in Figure 6 but under type 2 weather conditions.

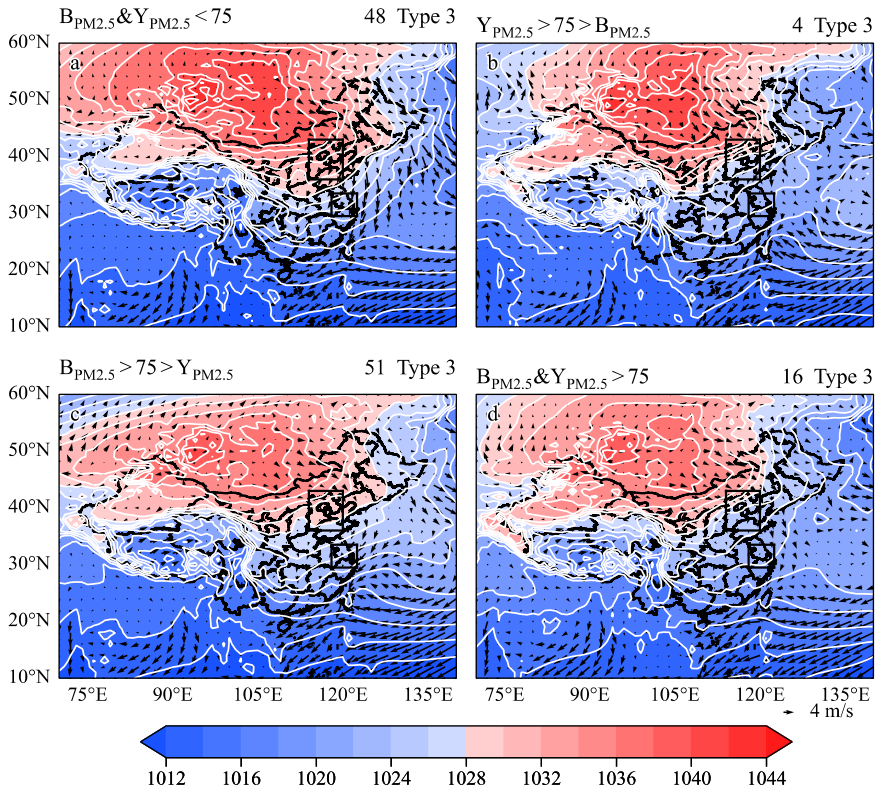


Figure 9. The sea level pressure field and 10 m wind field distribution with different $PM_{2.5}$ patterns under type 3 weather conditions: (**a**) $PM_{2.5}$ pattern I; (**b**) $PM_{2.5}$ pattern II; (**c**) $PM_{2.5}$ pattern III; (**d**) $PM_{2.5}$ pattern IV. The number at the top right corner of each panel indicates the number of days under each $PM_{2.5}$ pattern. The black frame area on the north side of each panel represents BTH, while the one on the south side represents YRD.

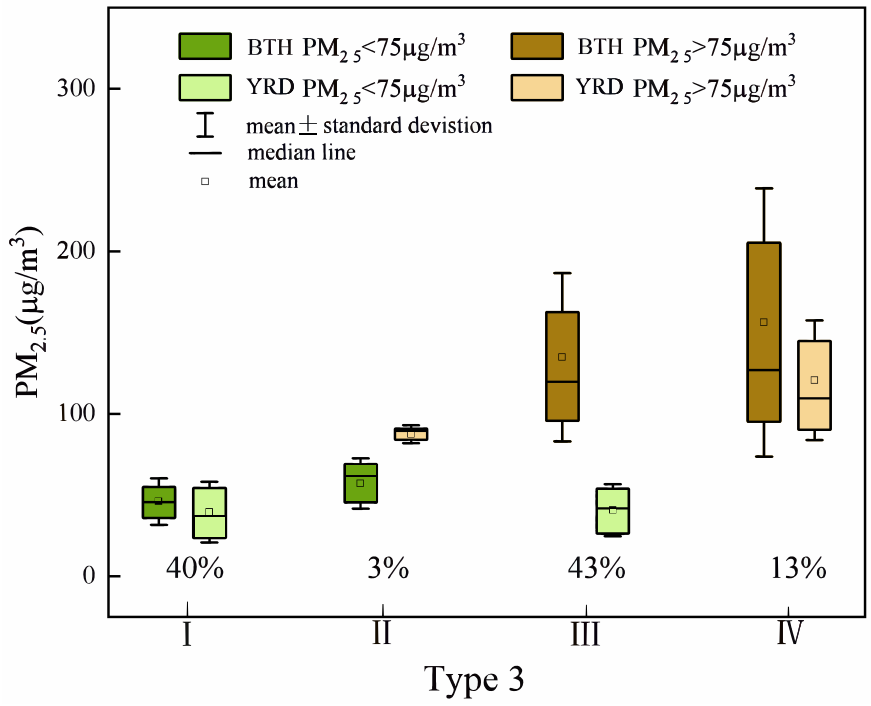


Figure 10. The same as in Figure 6 but under type 3 weather conditions.

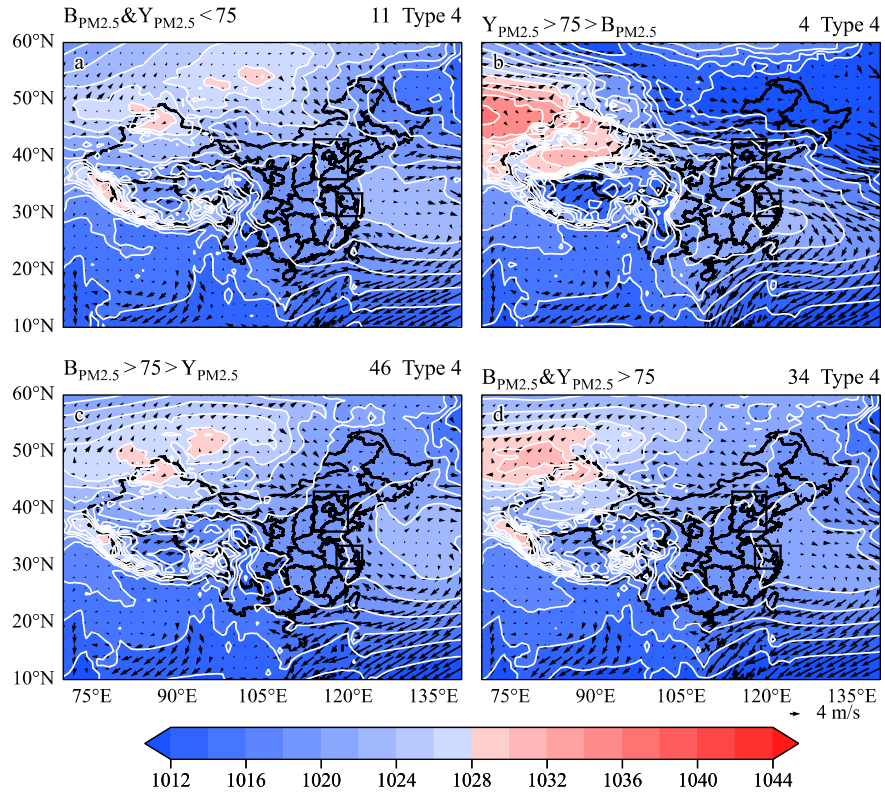


Figure 11. The sea level pressure field and 10 m wind field distribution with different $PM_{2.5}$ patterns under type 4 weather conditions: (**a**) $PM_{2.5}$ pattern I; (**b**) $PM_{2.5}$ pattern II; (**c**) $PM_{2.5}$ pattern III; (**d**) $PM_{2.5}$ pattern IV. The number at the top right corner of each panel indicates the number of days under each $PM_{2.5}$ pattern. The black frame area on the north side of each panel represents BTH, while the one on the south side represents YRD.

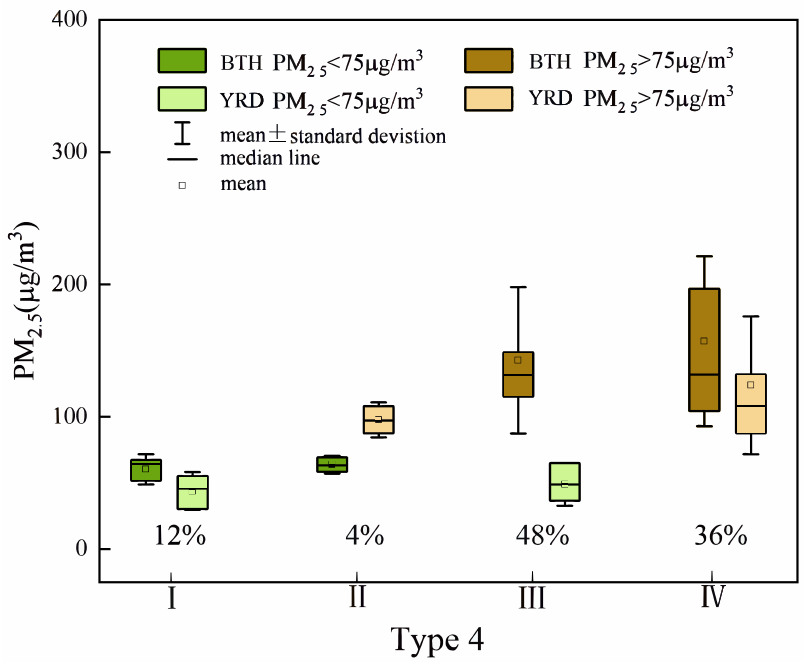


Figure 12. The same as in Figure 6 but under type 4 weather conditions.

Under type 1 weather conditions, the four $PM_{2.5}$ patterns accounted for 82, 57, 30 and 40 days, respectively. $PM_{2.5}$ pattern I occurred the most, usually accompanied by strong cold air. The sea level isobar at 1028 hPa was pressed south to approximately 28° N, and the whole ground in eastern China was controlled by high pressure, with strong surface winds. $PM_{2.5}$ concentrations were less than 50 μg/m^3 in both regions, and $PM_{2.5}$ concentrations in the YRD (46 μg/m^3) were slightly greater than those in BTH (39 μg/m^3) (Figures 5a and 6). The cold air of $PM_{2.5}$ pattern II was weaker than that of $PM_{2.5}$ pattern I, with the 1028 hPa sea level isobar reaching the west of BTH, and the cold air facilitated air pollutant dispersion with low $PM_{2.5}$ concentrations in BTH. However, air pollutants were transported to the YRD, causing pollution accumulation in the YRD. The average $PM_{2.5}$ concentrations were 47 and 106 μg/m^3 in BTH and the YRD, respectively (Figure 6). The weather conditions of $PM_{2.5}$ patterns III and IV were similar, with the 1028 hPa sea level isobar being located at the border between northern Hebei and Inner Mongolia, and the influence of cold air was very weak. The BTH region and YRD were under a uniform pressure system with weak winds. $PM_{2.5}$ concentrations in both regions mainly exhibited local accumulation.

Under type 2 weather conditions, $PM_{2.5}$ pattern III occurred the most, 82 days, accounting for 42%. $PM_{2.5}$ patterns I and IV occurred for 52 days and 51 days, respectively, while $PM_{2.5}$ pattern II occurred for the least amount of time, 15 days (Figure 7). The weather conditions of $PM_{2.5}$ pattern III were that BTH was located in the rear part of the split main body of the Mongolian high-pressure system and influenced by southerly airflow, resulting in an average $PM_{2.5}$ concentration of 128 μg/m^3 in BTH. Meanwhile, the YRD was in the front part of the split high-pressure system, controlled by strong easterly airflow, with a lower concentration of 48 μg/m^3 in YRD (Figures 7c and 8).

Similar to type 2, under type 3 weather conditions, $PM_{2.5}$ pattern III occurred the most, with 50 days (43%). Cold air passed through the northern BTH region, descending southward along the eastern path from the sea. In northern BTH, where isobars were dense and northwest winds were strong, pollutants dispersed easily. However, in central and southern BTH, the surface pressure field was weak, and the winds were low, leading to pollutant accumulation. The $PM_{2.5}$ concentration was 134 μg/m^3 in BTH, while in the YRD, influenced by clean airflows from the sea, the $PM_{2.5}$ concentration was 41 μg/m^3 (Figures 9c and 10). $PM_{2.5}$ pattern I accounted for 48 days (40%), and for this pattern, the Mongolian high pressure was relatively strong, with the central pressure intensity reaching

1040 hPa. The surface winds in BTH and the YRD were high, facilitating the dispersion of pollutants. The $PM_{2.5}$ concentrations in the two regions were low, being 46 and 39 μg/m^3, respectively (Figures 9a and 10).

Under type 4 weather conditions, the cold air was very weak. $PM_{2.5}$ pattern III occurred the most, with 46 days (48%), followed by $PM_{2.5}$ pattern IV, with 34 days (36%) (Figure 11). In $PM_{2.5}$ pattern III, BTH experienced uniform pressure, while the YRD was at the rear of high pressure over the Yellow Sea. Due to the strong southerly winds, the $PM_{2.5}$ concentration was low in the YRD, being 49 μg/m^3. Simultaneously, strong southerly winds facilitated the transport of air pollutants from BTH to the YRD, causing high $PM_{2.5}$ concentrations in BTH (146 μg/m^3) (Figures 11c and 12). If the high pressure over the Yellow Sea weakened, resulting in a weak surface wind, pollution would occur in the YRD, resulting in $PM_{2.5}$ pattern IV (Figure 11d).

3.3. Impact of Meteorological Factors on $PM_{2.5}$

3.3.1. Impact of Dynamic and Thermal Meteorological Factors on $PM_{2.5}$ in Two Regions

The significant differences in $PM_{2.5}$ concentrations between BTH and the YRD under different weather conditions are mainly due to variations in the meteorological factors that affect $PM_{2.5}$ diffusion. We compared the meteorological diffusion conditions in BTH and the YRD under different weather types. Figures 13 and 14 depict the boxplot statistics of regional averages for thermal and dynamic meteorological factors, respectively, under different weather conditions in BTH and the YRD.

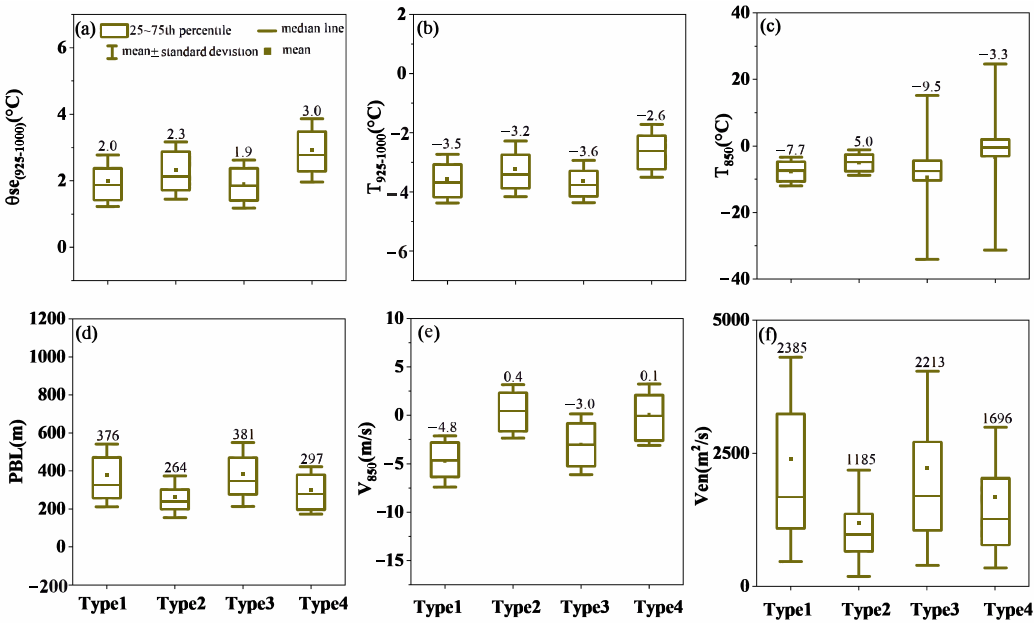


Figure 13. Boxplots of meteorological thermal and dynamic factors under different weather patterns in BTH: (**a**–**c**) represent the thermal factors $\theta_{se_925–1000}$, $T_{925–1000}$ and T_{850}; (**d**–**f**) represent the dynamic factors PBL, V_{850} and Ven. The number at the top of each box indicates the average of each meteorological factor.

The values of $\theta se_{_925–1000}$, $T_{925–1000}$, and T_{850} reflected the thermal state of the lower atmosphere, with larger values indicating a more stable lower atmospheric structure. The PBL and Ven reflected the dynamic state of the lower atmospheric layer. Larger values favored the turbulent mixing and vertical dispersion of air pollutants [37,38]. The V_{850} value was used as an indicator of the strength of the winter monsoon [33]. The stronger the northerly wind ($V_{850} < 0$), the stronger the winter monsoon. These factors can be used to evaluate the ability of air pollutants to disperse vertically.

For the thermal meteorological factors, in BTH, Figure 13 shows that the values of $\theta_{se_925–1000}$, $T_{925–1000}$, and T_{850} were the highest under type 4 weather conditions and were

slightly lower under type 2 weather conditions, indicating that the lower atmospheric structures were stable under type 2 and type 4 weather conditions. Under type 1 and type 3 weather conditions, the values of $\theta_{se_925–1000}$ were 2.0 and 1.9 °C, respectively, which were lower than those under type 2 and type 4 weather conditions. In the YRD, as shown in Figure 13, under type 4 weather conditions, similar to those in BTH, the values of $\theta_{se_925–1000}$, $T_{925–1000}$, and T_{850} were the highest, indicating the strongest stability in the lower atmospheric structure. Under type 3 weather conditions, the YRD exhibited high values of these three thermal factors, demonstrating strong thermal stability in the lower atmosphere, which was different from that in BTH. Under type 1 or type 2 weather conditions, the values of $\theta_{se_925–1000}$, $T_{925–1000}$, and T_{850} were relatively low, indicating weaker stability in the lower atmospheric structure in the YRD. Therefore, in both BTH and the YRD, the lower atmospheric structure was unstable under type 1 conditions and stable under type 4 conditions. The type 2 and type 3 conditions have different stabilities for the lower atmospheric structures in these two regions. For example, under type 2, the atmospheric structure in BTH was stable (the average value of $\theta_{se_925–1000}$ was 2.3 °C), while that in the YRD was weak (the average value of $\theta_{se_925–1000}$ was 0.9 °C). The atmospheric structure of BTH decreased from strong to weak (type 4, type 2, type 1 and type 3), while that of the YRD decreased in the order of type 4, type 3, type 2 and type 1.

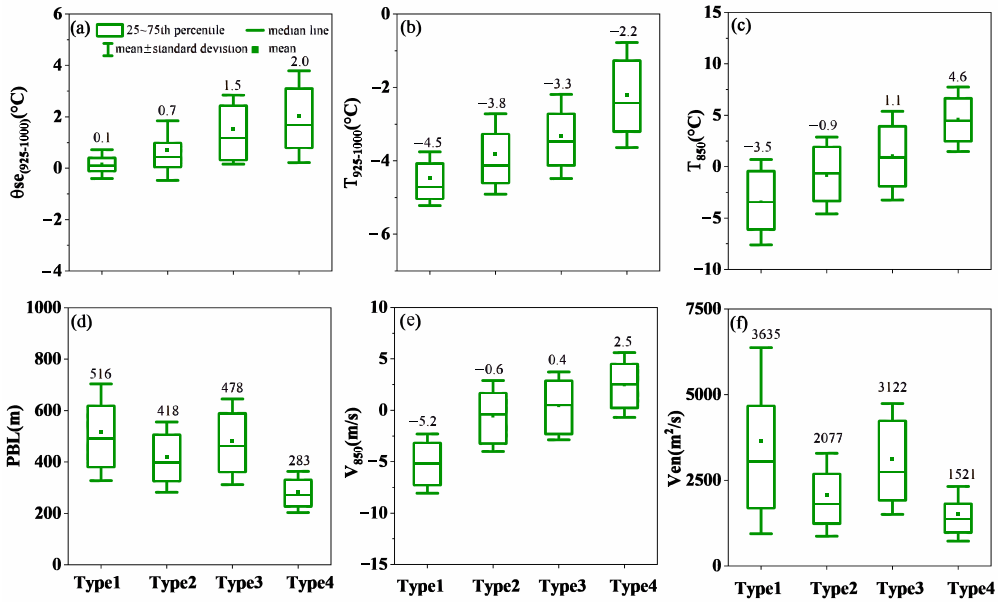


Figure 14. Boxplots of meteorological thermal and dynamic factors under different weather patterns in the YRD: (**a**–**c**) represent the thermal factors $\theta_{se_925–1000}$, $T_{925–1000}$ and T_{850}; (**d**–**f**) represent the dynamic factors PBL, V_{850} and Ven. The number at the top of each box indicates the average of each meteorological factor.

For the dynamic meteorological factors, in BTH (Figure 13d–f), under type 1 or type 3 weather conditions, the PBL and Ven were high, and the average values reached more than 300 m and 2000 m^2/s, respectively. The V_{850} was a strong northerly wind with average speeds exceeding −3 m/s. However, under type 2 and type 4 weather conditions, the PBL and Ven were low, and V_{850} was a weak southerly wind (value of V_{850} < 0.5 m/s), which was conducive to transporting air pollutants from the southern region to the BTH region. Warm and humid airflows carrying air pollutants accumulate in front of mountains, increasing humidity and hindering pollutant dispersion. Figure 14d–f shows that under type 1 weather conditions in the YRD, the average PBL and Ven were the highest, being 516 m and 3635 m^2/s, respectively, and V_{850} was a strong northerly wind (−5.2 m/s). PBL and Ven were lowest under type 4 weather conditions, being 283 m and 1152 m^2/s, respectively, and V_{850} was a southerly wind (2.5 m/s). Therefore, for BTH, under type

1 or type 3 (type 2 or type 4) weather conditions, the vertical dispersion of air pollutants was favorable (unfavorable). However, in the YRD, only type 4 exhibited poor vertical dispersion of air pollutants, with dispersion decreasing from strong to weak in the order of type 1, type 3, type 2, and type 4.

Considering both thermal and dynamic factors, for BTH, the dispersion conditions of air pollutants were poor under type 2 and type 4 weather conditions, leading to the accumulation of pollutants near the surface. This was the main reason for the heavy pollution in BTH under these two weather conditions. For the YRD, the type 4 weather conditions were similar to those in BTH, and the high $PM_{2.5}$ concentration was mainly caused by stable weather. However, under type 1 weather conditions, the vertical dispersion of pollutants was strongest, yet the $PM_{2.5}$ concentration was high. Although the PBL was high, the air pollutants from the NCP were easily transported to the YRD by strong northerly winds, causing pollution in the YRD.

3.3.2. Impacts of Dynamic and Thermal Meteorological Factors on $PM_{2.5}$ Pollution Levels

To analyze the impacts of meteorological factors on $PM_{2.5}$ pollution levels in the two study regions, Tables 1 and 2 provide the mean values of meteorological factors for light, moderate and severe pollution under different weather types. In comparing Tables 1 and 2, there were differences in $PM_{2.5}$ pollution levels and meteorological factors between BTH and the YRD under different weather conditions. Regardless of the weather conditions, the frequency of moderate and severe pollution in BTH was significantly greater than that in the YRD.

Table 1. Average meteorological factors at the three pollution levels under the four weather types in BTH.

Weather Types	Pollution Level	$PM_{2.5}$ ($\mu g/m^3$)	P ($PM_{2.5}$) (%)	$\theta_{se_925–1000}$ (°C)	$T_{925–1000}$ (°C)	T_{850} (°C)	PBL (m)	V_{850} (m/s)	Ven (m^2/s)
Type1	light	88.4	16.8	2.3	−3.2	−5.4	326.7	−3.2	1878.9
	moderate	136.3	10.1	2.6	−2.7	−4.3	283.8	−4.1	1550.3
	severe	194.0	6.7	2.7	−2.4	−2.8	248.5	−2.9	1451.7
Type2	light	93.7	27.2	2.4	−3.2	−4.9	251.9	0.5	1127.3
	moderate	133.2	14.9	2.5	−3.0	−3.3	222.9	1.0	898.9
	severe	211.4	24.8	2.5	−2.8	−3.7	221.7	0.8	951.1
Type3	light	93.3	26.9	1.8	−3.7	−7.9	397.0	−3.3	2478.0
	moderate	136.3	10.1	2.6	−3.0	−3.8	320.8	−1.6	1788.5
	severe	206.5	19.3	2.3	−3.2	−3.5	257.9	−1.6	1233.5
Type4	light	93.5	23.2	2.5	−2.9	−2.4	311.8	−0.9	1792.3
	moderate	131.6	34.7	3.0	−2.6	0.0	321.4	0.2	1938.7
	severe	220.0	26.3	3.4	−2.0	1.3	223.3	0.9	1197.1

P ($PM_{2.5}$): the frequency of $PM_{2.5}$ pollution levels under different weather types.

Table 1 shows that there was little difference in the frequency of light pollution; however, it varied significantly between moderate and severe pollution in BTH under different weather conditions. Moderate and severe pollution occurred most frequently in type 4 conditions, followed by type 2 and type 3, and type 1 conditions had the lowest pollution, with frequencies of 61.0%, 39.7%, 29.4% and 16.8%, respectively; additionally, the corresponding average $PM_{2.5}$ concentrations for severe pollution were 220.0, 211.4, 206.5, and 194.0 $\mu g/m^3$, respectively. Under type 4 weather conditions, the thermal meteorological factors for moderate and severe pollution were high. For example, the values of $\theta_{se_925–1000}$ and T_{850} reached 3.4 °C and 1.3 °C, respectively, indicating that a stable lower atmospheric thermal structure was unfavorable for the vertical mixing of pollutants. Moreover, the PBL was low, with V_{850} being in a near-calm state (0.2 m/s). The thermal and dynamic factors in type 4 weather created favorable conditions for the occurrence of moderate and severe pollution. Under type 2 weather conditions, the frequency of severe pollution

reached 24.8%, second only to type 4 (26.3%). Type 2 was also an important weather pattern conducive to severe pollution in BTH.

Table 2. Average meteorological factors at the three pollution levels under the four weather types in the YRD.

Weather Types	Pollution Level	$PM_{2.5}$ ($\mu g/m^3$)	P ($PM_{2.5}$) (%)	$\theta_{se_925–1000}$ (°C)	$T_{925–1000}$ (°C)	T_{850} (°C)	PBL (m)	V_{850} (m/s)	Ven (m^2/s)
Type1	light	90.8	30.1	0.1	−4.3	−1.4	472.0	−4.7	3114.9
	moderate	127.6	9.6	0.2	−4.2	−2.5	419.5	−4.8	2707.0
	severe	190.0	6.7	−0.1	−4.1	−1.3	454.6	−4.4	3100.2
Type2	light	91.0	23.8	0.6	−3.6	0.3	360.4	−1.1	1660.9
	moderate	128.7	6.9	1.2	−3.3	0.6	346.3	−1.1	1549.6
	severe	181.0	2.0	−0.3	−3.6	−1.3	348.1	−4.5	1556.0
Type3	light	91.8	10.9	1.2	−3.4	1.4	393.1	0.1	2366.5
	moderate	137.3	3.4	2.9	−2.7	5.2	368.2	−0.3	2418.7
	severe	179.1	2.5	1.5	−3.0	2.1	318.9	−0.7	1454.8
Type4	light	94.3	25.3	1.2	−2.6	3.7	287.5	0.7	1537.4
	moderate	129.2	8.4	2.4	−1.6	5.3	251.0	1.8	1508.3
	severe	216.9	6.3	2.9	−1.5	7.5	260.4	2.4	1071.9

P ($PM_{2.5}$): the frequency of $PM_{2.5}$ pollution levels under different weather types.

As shown in Table 2, unlike BTH, the YRD exhibited a significantly greater occurrence of light pollution than moderate or severe pollution. Additionally, the frequency of light pollution varied notably according to weather pattern, with type 1 conditions showing the highest frequency, followed by type 4 and type 2, with type 3 conditions having the lowest frequency; the frequencies were 30.1%, 25.3%, 23.8% and 10.1%, with corresponding average $PM_{2.5}$ concentrations of 90.8, 94.3, 91.0 and 91.8 $\mu g/m^3$, respectively. However, under type 1 weather conditions, the frequencies of different pollution levels were greater than those under type 4 weather conditions, and the corresponding average $PM_{2.5}$ concentration was lower than that under type 4 weather conditions. Therefore, both type 1 and type 4 weather patterns are important weather patterns that contribute to pollution events in the YRD.

4. Discussion

The $PM_{2.5}$ concentration was still high in eastern China, especially in BTH and the YRD. Understanding the meteorological conditions affecting $PM_{2.5}$ pollution in these two areas has important guiding significance for the prevention and control of pollution events. In this study, we analyzed the main weather conditions affecting eastern China from the winters of 2013 to 2019 and compared the $PM_{2.5}$ variations in the winters in BTH and the YRD under different weather conditions, as well as the differences in the thermal and dynamic factors affecting the $PM_{2.5}$ concentration. The results showed that meteorological conditions had different impacts on $PM_{2.5}$ variation in BTH and the YRD. In BTH, the probability of heavy $PM_{2.5}$ pollution in stable weather was high (26.3%), while that in the YRD was high (6.7%) under the transport weather conditions (strong northerly winds), indicating that the impact of pollutant transportation in the YRD area was more obvious than that in stable weather. Notably, in this study, we did not compare the impact of meteorological conditions on primary and secondary $PM_{2.5}$ or $PM_{2.5}$ chemical compositions in BTH and the YRD. Huang et al. [32] revealed that the precursors for secondary $PM_{2.5}$ from the YRD can be transported to BTH under southerly winds and under favorable weather conditions, similar to the aqueous-phase and heterogeneous chemical production of secondary aerosols in BTH, and then the strong northerly winds can transport the primary and secondary $PM_{2.5}$ back to the YRD. Therefore, we will further explore the effects of weather conditions on primary and secondary $PM_{2.5}$ and $PM_{2.5}$ chemical compositions in these two regions based on satellite remote sensing data.

5. Conclusions

Fine particulate pollution still occurred in winter in eastern China, including in BTH and the YRD. Meteorological conditions are important factors for determining $PM_{2.5}$ pollution. In this study, the T-PCA method from the Cost733 model was used to objectively classify the sea level pressure field and 10 m wind field in the eastern part of China (20–50° N, 100–130° E) during winters from 2013 to 2019. Four weather types were identified, and their influences on the $PM_{2.5}$ distribution across BTH and the YRD were explored. The main conclusions of this study are described as follows:

(1) Type 1 conditions were the most common weather type during winter, occurring on 210 days. In type 1 weather conditions, which are affected by high pressure moving eastward and southward, air pollutants are transported from north to south. In type 2 weather conditions, the weak high pressure moved southward, the cold air pressure was weak, and BTH was located at the back of the high pressure zone, which is conducive to $PM_{2.5}$ pollution. Under type 3 weather conditions, cold air flows southward along the east side of the road, which is beneficial for pollutant diffusion across BTH and the YRD. During type 4 weather conditions, there was no significant cold air activity, and most areas in eastern China were affected by southerly airflow behind the high-pressure system over the Yellow Sea. These stable weather conditions were a major contributor to heavy pollution events in BTH and the YRD.

(2) For BTH, type 2 and type 4 conditions were the main weather conditions leading to high $PM_{2.5}$ concentrations. In type 2 and type 4 weather conditions, the atmospheric vertical mixing was poor, leading to the accumulation of pollutants near the surface. Compared to those under type 2 conditions, under type 4 conditions, the values of $\theta_{se_925–1000}$, $T_{925–1000}$ and T_{850} were greater, while the PBL and Ven were lower, providing more favorable conditions for moderate and severe pollution. Under type 1 and type 3 conditions, cold air moves southward or eastward along the path, creating favorable thermal and dynamic dispersion conditions for $PM_{2.5}$ removal in this region.

(3) For the YRD, type 1 and type 4 conditions were the main weather conditions leading to high $PM_{2.5}$ concentrations, with type 1 conditions having higher frequencies of pollution events but lower concentrations than type 4 conditions. Type 1 favored the transport of pollutants from north to south, leading to varying degrees of $PM_{2.5}$ pollution in the YRD. Under type 4 conditions, the PBL and Ven were the lowest, significantly reducing the vertical mixing and dispersion of air pollutants and facilitating the occurrence of severe pollution. Under type 2 and type 3 conditions, the PBL and Ven increased, resulting in less $PM_{2.5}$ pollution.

Author Contributions: X.L. wrote and revised the manuscript, analyzed the data, and generated the figures. H.W. designed the research, and Y.Z. and P.W. downloaded the $PM_{2.5}$ and meteorological data. All the authors polished this paper. All authors have read and agreed to the published version of the manuscript.

Funding: This research was funded by the Jiangsu Key Laboratory of Atmospheric Environment Monitoring and Pollution Control (KHK2205) and the National Natural Science Foundation of China (Grant No. 52331012).

Institutional Review Board Statement: Not applicable.

Informed Consent Statement: Not applicable.

Data Availability Statement: The $PM_{2.5}$ data were obtained from a high-resolution and high-quality ambient air pollutant dataset for China (https://weijing-rs.github.io/product.html) (accessed on 1 January 2024). The ERA-5 hourly data on pressure levels and single levels were downloaded from https://doi.org/10.24381/cds.bd0915c6 and https://doi.org/10.24381/cds.adbb2d47 (accessed on 1 January 2024), respectively.

Conflicts of Interest: The authors declare no conflicts of interest.

References

1. He, J.J.; Gong, S.L.; Liu, H.L.; An, X.Q.; Yu, Y.; Zhao, S.P.; Wu, L.; Song, C.B.; Zhou, C.H.; Wang, J. Influences of meteorological conditions on interannual variations of particulate matter pollution during winter in the Beijing–Tianjin–Hebei area. *Meteorol. Res.* **2017**, *31*, 1062–1069. [CrossRef]
2. Fu, G.Q.; Xu, W.Y.; Yang, R.F.; Li, J.B.; Zhao, C.S. The distribution and trends of fog and haze in the North China Plain over the past 30 years. *Atmos. Chem. Phys.* **2014**, *14*, 11949–11958. [CrossRef]
3. Ning, G.C.; Wang, S.G.; Yim, S.H.L.; Li, J.; Hu, Y.; Shang, Z.; Wang, J.; Wang, J. Impact of low-pressure systems on winter heavy air pollution in the northwest Sichuan Basin, China. *Atmos. Chem. Phys.* **2018**, *18*, 13601–13615. [CrossRef]
4. Gao, M.; Carmichael, G.R.; Wang, Y.; Saide, P.E.; Yu, M.; Xin, J.; Liu, Z.; Wang, Z. Modeling study of the 2010 regional haze event in the North China Plain. *Atmos. Chem. Phys.* **2016**, *16*, 1673–1691. [CrossRef]
5. Huang, R.J.; Zhang, Y.; Bozzetti, C.; Ho, K.F.; Cao, J.J.; Han, Y.; Daellenbach, K.R.; Slowik, J.G.; Platt, S.M.; Canonaco, F.; et al. High secondary aerosol contribution to particulate pollution during haze events in China. *Nature* **2014**, *514*, 218–222. [CrossRef]
6. Chen, H.; Wang, H.; Sun, J.; Xu, Y.; Yin, Z. Anthropogenic fine particulate matter pollution will be exacerbated in eastern China due to 21st century GHG warming. *Atmos. Chem. Phys.* **2019**, *19*, 233–243. [CrossRef]
7. Lu, X.; Lin, C.; Li, W.; Chen, Y.; Huang, Y.; Fung, J.C.H.; Lau, A.K.H. Analysis of the adverse health effects of $PM_{2.5}$ from 2001 to 2017 in China and the role of urbanization in aggravating the health burden. *Sci. Total Environ.* **2019**, *652*, 683–695. [CrossRef]
8. Lelieveld, J.; Evans, J.S.; Fnais, M.; Giannadaki, D.; Pozzer, A. The contribution of outdoor air pollution sources to premature mortality on a global scale. *Nature* **2015**, *525*, 367–371. [CrossRef] [PubMed]
9. Geng, G.; Xiao, Q.; Zheng, Y.; Tong, D.; Zhang, Y.; Zhang, X.; Zhang, Q.; He, K.; Liu, Y. Impact of China's air pollu-tion prevention and control action plan on $PM_{2.5}$ chemical composition over eastern China. *Sci. China Earth Sci.* **2019**, *62*, 1872–1884. [CrossRef]
10. Zheng, Y.; Xue, T.; Zhang, Q.; Geng, G.; Tong, D.; Li, X.; He, K. Air quality improvements and health benefits from China's clean air action since 2013. *Environ. Res. Lett.* **2017**, *12*, 114020. [CrossRef]
11. Wang, Y.; Gao, W.; Wang, S.; Song, T.; Gong, Z.; Ji, D.; Wang, L.; Liu, Z.; Tang, G.; Huo, Y. Contrasting trends of $PM_{2.5}$ and surface-ozone concentrations in China from 2013 to 2017. *Natl. Sci. Rev.* **2020**, *7*, 1331–1339. [CrossRef] [PubMed]
12. Ding, A.; Huang, X.; Nie, W.; Chi, X.; Xu, Z.; Zheng, L.; Xu, Z.; Xie, Y.; Qi, X.; Shen, Y.; et al. Significant reduction of $PM_{2.5}$ in eastern China due to regional-scale emission control: Evidence from SORPES in 2011–2018. *Atmos. Chem. Phys.* **2019**, *19*, 11791–11801. [CrossRef]
13. Huang, X.; Ding, A.J.; Gao, J.; Zheng, B.; Zhou, D.R.; Qi, X.M.; Tang, R.; Wang, J.P.; Ren, C.; Nie, W.; et al. Enhanced secondary pollution offset reduction of primary emissions during COVID-19 lockdown in China. *Natl. Sci. Rev.* **2021**, *8*, nwaa137. [CrossRef] [PubMed]
14. She, Q.; Choi, M.; Belle, J.H.; Xiao, Q.; Bi, J.; Huang, K.; Meng, X.; Geng, G.; Kim, J.; He, K.; et al. Satel-lite-based estimation of hourly $PM_{2.5}$ levels during heavy winter pollution episodes in the Yangtze River Delta, China. *Chemosphere* **2020**, *239*, 124678. [CrossRef] [PubMed]
15. An, Z.S.; Huang, R.J.; Zhang, R.Y.; Tie, X.X.; Li, G.H.; Cao, J.J.; Zhou, W.J.; Shi, Z.; Han, Y.; Gu, Z.; et al. Severe haze in northern China: A synergy of anthropogenic emissions and atmospheric processes. *Proc. Natl. Acad. Sci. USA* **2019**, *116*, 8657–8666. [CrossRef] [PubMed]
16. Cai, W.J.; Li, K.; Liao, H.; Wang, H.J.; Wu, L.X. Weather conditions conducive to Beijing severe haze more frequent under climate change. *Nat. Clim. Chang.* **2017**, *7*, 257–262. [CrossRef]
17. Liu, X.H.; Zhu, B.; Kang, H.Q.; Hou, X.W.; Gao, J.; Kuang, X.; Yan, S.; Shi, S.; Fang, C.; Pan, C.; et al. Stable and transport indices applied to winter air pollution over the Yangtze River Delta, China. *Environ. Pollut.* **2021**, *272*, 115954. [CrossRef] [PubMed]
18. Ye, X.; Song, Y.; Cai, X.; Zhang, H. Study on the synoptic flow patterns and boundary layer process of the severe haze events over the North China Plain in January 2013. *Atmos. Environ.* **2016**, *124*, 129–145. [CrossRef]
19. Jia, B.; Wang, Y.; Yao, Y.; Xie, Y. A new indicator on the impact of large-scale circulation on wintertime particulate matter pollution over China. *Atmos. Chem. Phys.* **2015**, *15*, 11919–11929. [CrossRef]
20. Huang, X.; Wang, Z.; Ding, A. Impact of aerosol-PBL interaction on haze pollution: Multiyear observational evidence in North China. *Geophys. Res. Lett.* **2018**, *45*, 8596–8603. [CrossRef]
21. Quan, J.; Tie, X.; Zhang, Q.; Liu, Q.; Li, X.; Gao, Y.; Zhao, D. Characteristics of heavy aerosol pollution during the 2012-2013 winter in Beijing, China. *Atmos. Environ.* **2014**, *88*, 83–89. [CrossRef]
22. Zhu, X.W.; Tang, G.Q.; Guo, J.P.; Hu, B.; Song, T.; Wang, L.L.; Xin, J.Y.; Gao, W.K.; Münkel, C.; Schäfer, K.; et al. Mixing layer height on the North China Plain and meteorological evidence of serious air pollution in southern Hebei. *Atmos. Chem. Phys.* **2018**, *18*, 4897–4910. [CrossRef]
23. Hou, X.W.; Fei, D.D.; Kang, H.Q.; Zhang, Y.L.; Gao, J.H. Seasonal statistical analysis of the impact of meteoro-logical factors on fine particle pollution in China in 2013-2017. *Nat. Hazards* **2018**, *93*, 677–698. [CrossRef]
24. Luan, T.; Guo, X.; Guo, L.; Zhang, T. Quantifying the relationship between $PM_{2.5}$ concentration, visibility and planetary boundary layer height for long-lasting haze and fog-haze mixed events in Beijing. *Atmos. Chem. Phys.* **2018**, *18*, 203–225. [CrossRef]
25. Wang, J.; Wang, S.; Jiang, J.; Ding, A.; Zheng, M.; Zhao, B.; Wong, D.C.; Zhou, W.; Zheng, G.; Wang, L.; et al. Impact of aerosol-meteorology interactions on fine particle pollution during China's severe haze episode in January 2013. *Environ. Res. Lett.* **2014**, *9*, 094002. [CrossRef]

26. Hou, X.W.; Zhu, B.; Kumar, K.R.; de Leeuw, G.; Lu, W.; Huang, Q.; Zhu, X.X. Establishment of Conceptual Schemas of Surface Synoptic Meteorological Situations Affecting Fine Particulate Pollution Across Eastern China in the Winter. *J. Geophys. Res. Atmos.* **2020**, *125*, e2020JD033153. [CrossRef]
27. Zhang, W.H.; Hai, S.F.; Zhao, Y.H.; Sheng, L.F.; Zhou, Y.; Wang, W.C.; Li, W.S. Numerical modeling of regional transport of $PM_{2.5}$ during a severe pollution event in the Beijing-Tianjin-Hebei Region in November 2015. *Atmos. Environ.* **2021**, *254*, 118393. [CrossRef]
28. Li, J.; Du, H.Y.; Wang, Z.F.; Sun, Y.L.; Yang, W.Y.; Li, J.J.; Tang, X.; Fu, P.Q. Rapid formation of a severe regional winter haze episode over a mega-city cluster on the North China Plain. *Environ. Pollut.* **2017**, *223*, 605–615. [CrossRef]
29. Wu, P.; Ding, Y.H.; Liu, Y.J. Atmospheric circulation and dynamic mechanism for persistent haze events in the Beijing-Tianjin-Hebei Region. *Adv. Atmos. Sci.* **2017**, *34*, 429–440. [CrossRef]
30. Ding, Y.H.; Wu, P.; Liu, Y.J.; Song, Y. Environmental and dynamic conditions for the occurrence of persistent haze events in North China. *Engineering* **2017**, *3*, 266–271. [CrossRef]
31. Kang, H.Q.; Zhu, B.; Liu, X.H.; Shi, S.S.; Hou, X.W.; Lu, W.; Yan, S.; Pan, C.; Chen, Y. Three-Dimensional Distribution of $PM_{2.5}$ over the Yangtze River Delta as Cold Fronts Moving Through. *J. Geophys. Res. Atmos.* **2021**, *126*, e2020JD034035. [CrossRef]
32. Huang, X.; Ding, A.J.; Wang, Z.L.; Ding, K.; Gao, J.; Chai, F.H.; Fu, C.B. Amplified transboundary transport of haze by aerosol boundary layer interaction in China. *Nat. Geosci.* **2020**, *13*, 428–434. [CrossRef]
33. Liu, X.H.; Zhu, B.; Zhu, T.; Liao, H. The seesaw pattern of $PM_{2.5}$ interannual anomalies between Beijing Tian-jin-Hebei and Yangtze River Delta across eastern China in winter. *Geophys. Res. Lett.* **2022**, *49*, e2021GL095878. [CrossRef]
34. Wei, J.; Li, Z.; Lyapustin, A.; Sun, L.; Peng, Y.R.; Xue, W.H.; Su, T.N.; Cribb, M. Reconstructing 1-km-resolution high-quality $PM_{2.5}$ data records from 2000 to 2018 in China: Spatiotemporal variations and policy implications. *Remote Sens. Environ.* **2021**, *252*, 112136. [CrossRef]
35. Huth, R.; Beck, C.; Philipp, A.; Demuzere, M.; Ustrnul, Z.; Cahynová, M.; Kyselý, J.; Tveito, O.E. Classifications of atmospheric circulation patterns:recent advances and applications. *Trends Dir. Clim. Res.* **2008**, *1146*, 105–152. [CrossRef]
36. Huth, R. A circulation classification scheme applicable in GCM studies. *Theor. Appl. Climatol.* **2000**, *67*, 1–18. [CrossRef]
37. Ji, D.S.; Wang, Y.S.; Wang, L.L.; Chen, L.; Hu, B.; Tang, G.; Xin, J.; Song, T.; Wen, T.; Sun, Y.; et al. Analysis of heavy pollution episodes in selected cities of Northern China. *Atmos. Environ.* **2012**, *50*, 338–348. [CrossRef]
38. Quan, J.N.; Gao, Y.; Zhang, Q.; Tie, X.X.; Cao, J.; Han, S.; Meng, J.; Chen, P.; Zhao, D. Evolution of planetary boundary layer under different weather conditions, and its impact on aerosol concentrations. *Particuology* **2013**, *11*, 34–40. [CrossRef]

Disclaimer/Publisher's Note: The statements, opinions and data contained in all publications are solely those of the individual author(s) and contributor(s) and not of MDPI and/or the editor(s). MDPI and/or the editor(s) disclaim responsibility for any injury to people or property resulting from any ideas, methods, instructions or products referred to in the content.